[CANCER RESEARCH 64, 8604–8612, December 1, 2004]

CXCR4 Regulates Growth of Both Primary and Metastatic Breast Cancer

Matthew C. P. Smith,[1] Kathryn E. Luker,[1] Joel R. Garbow,[3] Julie L. Prior,[1] Erin Jackson,[1] David Piwnica-Worms,[1,2] and Gary D. Luker[1]

[1]Molecular Imaging Center, Mallinckrodt Institute of Radiology, and [2]Department of Molecular Biology and Pharmacology, Washington University School of Medicine, St. Louis, Missouri; and [3]Department of Chemistry, Washington University, St. Louis, Missouri

ABSTRACT

The chemokine receptor CXCR4 and its cognate ligand CXCL12 recently have been proposed to regulate the directional trafficking and invasion of breast cancer cells to sites of metastases. However, effects of CXCR4 on the growth of primary breast cancer tumors and established metastases and survival have not been determined. We used stable RNAi to reduce expression of CXCR4 in murine 4T1 cells, a highly metastatic mammary cancer cell line that is a model for stage IV human breast cancer. Using noninvasive bioluminescence and magnetic resonance imaging, we showed that knockdown of CXCR4 significantly limited the growth of orthotopically transplanted breast cancer cells. Mice in which parental 4T1 cells were implanted had progressively enlarging tumors that spontaneously metastasized, and these animals all died from metastatic disease. Remarkably, RNAi of CXCR4 prevented primary tumor formation in some mice, and all mice transplanted with CXCR RNAi cells survived without developing macroscopic metastases. To analyze effects of CXCR4 on metastases to the lung, an organ commonly affected by metastatic breast cancer, we injected tumor cells intravenously and monitored cell growth with bioluminescence imaging. Inhibiting CXCR4 with RNAi, or the specific antagonist AMD3100, substantially delayed the growth of 4T1 cells in the lung, although neither RNAi nor AMD3100 prolonged overall survival in mice with experimental lung metastases. These data indicate that CXCR4 is required to initiate proliferation and/or promote survival of breast cancer cells *in vivo* and suggest that CXCR4 inhibitors will improve treatment of patients with primary and metastatic breast cancer.

INTRODUCTION

Breast cancer is the most common malignant disease in Western women, and metastases are the cause of almost all cancer deaths (1). Breast cancer metastases most commonly occur in regional lymph nodes, lung, liver, and bone. These organ-selective sites of breast cancer metastases cannot be attributed solely to patterns of blood flow (2). However, mechanisms that regulate the multistep progression from primary tumor to trafficking and survival of cancer cells in selected organs remain poorly defined.

Recent studies suggest that the chemokine receptor CXCR4 is an important regulator of breast cancer metastases. Analogous to directed homing of leukocytes, gradients of the chemokine CXCL12, the chemotactic ligand for CXCR4, are proposed to attract tumor cells and regulate proliferation and invasion at specific metastatic sites (3–5). High levels of CXCL12 are produced in sites commonly affected by breast cancer metastases, and expression of the cognate receptor CXCR4 is higher in premalignant breast epithelium and breast cancer cells compared with normal breast epithelium (3, 6, 7). In severe combined immunodeficient mouse models of breast cancer, a polypeptide antagonist to CXCR4 significantly reduced growth of intravenously injected cancer cells in lung (8), and experimental and spontaneous breast cancer metastases both were reduced with a neutralizing antibody to CXCR4 (3). CXCR4 also appears to regulate metastases of other cancer types, as evidenced by a requirement for CXCR4 in the initial proliferation of colon cancer cells in the lung after the intravenous injection of tumor cells (9).

Expression of CXCR4 appears to be regulated by the tumor environment *in vivo*. Amounts of CXCR4 at the cell surface increased in breast cancer cells that were recovered and expanded from mammary fat pad xenografts in nude mice compared with parental cells in culture (10). Additional increases in CXCR4 expression were detected in tumor cells derived from spontaneous lung metastases. After left ventricular injection of breast cancer cells in nude mice, CXCR4 was among a small number of molecules that promoted bone metastases (11). Overexpression of CXCR4 alone in breast cancer cells also produced small increases in experimentally produced bone metastases. Although these data further support a function of CXCR4 in metastatic breast cancer, the studies may be limited by the use of immunocompromised mouse models. This is an important consideration because CXCR4 regulates normal lymphocyte trafficking, and CXCR4 signaling in the tumor microenvironment recruits plasmacytoid dendritic cells that suppress T-cell–mediated antitumor immunity (12). Therefore, immunocompromised mice may not appropriately reproduce interactions between normal host tissues and cancer cells that regulate breast cancer progression *in vivo* (7).

In addition to functions in metastatic cancer, studies with other cell types indicate that CXCR4 may affect proliferation and survival in the primary cellular environment. Administration of neutralizing antibodies to CXCR4 decreased proliferation and increased apoptosis in pancreatic ductal cells from diabetes-prone nonobese diabetic (NOD) mice (13). Pharmacological inhibition of CXCR4 produced similar effects on tumor cell growth and survival in orthotopic xenografts of brain tumors into nude mice (14). Although these data show that CXCR4 affects cell proliferation in normal tissue environments, it is unknown whether CXCR4 functions in the growth and progression of primary breast cancers.

We used noninvasive molecular imaging techniques to investigate CXCR4 in an immunocompetent mouse model of primary and metastatic breast cancer. When orthotopically transplanted to mammary fat pad, 4T1 breast cancer cells spontaneously metastasize in BALB/c mice, thereby reproducing many features of human breast cancer (15). Using stable RNA interference (RNAi) to reduce expression of CXCR4 in 4T1 cells, we show that CXCR4 is necessary for the growth and metastasis of orthotopically implanted tumor cells. The initial growth of experimentally produced lung metastases also is delayed by RNAi of CXCR4 or pharmacological inhibition with the specific CXCR4 antagonist AMD3100 (16). These data support the clinical use of CXCR4 antagonists in therapy of primary and metastatic breast cancer.

Received 5/26/04; revised 9/15/04; accepted 9/3/04.

Grant support: This study was funded by NIH grant P50 CA94056, Department of Defense grant BC023394, and NIH grant 1 R24 CA83060 to the Small Animal Imaging Resource Program at Washington University.

The costs of publication of this article were defrayed in part by the payment of page charges. This article must therefore be hereby marked *advertisement* in accordance with 18 U.S.C. Section 1734 solely to indicate this fact.

Note: M. Smith, K. Luker, and G. Luker are currently in the Department of Radiology, University of Michigan Medical School, Ann Arbor, Michigan.

Requests for reprints: Gary D. Luker, Department of Radiology, University of Michigan Medical School, 1150 West Medical Center Drive, Room 9303 MSRB III, Ann Arbor, MI 48109-0648. Phone: (734)-763-5849; Fax: (734)-647-2563; E-mail: gluker@umich.edu.

MATERIALS AND METHODS

Cells and DNA Constructs. 4T1 cells, a breast cancer cell line derived from a BALB/c mouse, were obtained from the American Type Culture Collection (Manassas, VA) and cultured in DMEM, 10% heat-inactivated fetal bovine serum, 1% glutamine, 0.1% fungizone, and 0.1% penicillin/streptomycin. 293T cells were cultured in the same medium.

To construct a lentiviral vector that expresses both firefly luciferase (FL) and enhanced green fluorescent protein (EGFP), we removed the human EF-1α promoter from pBudCE4.1 (Invitrogen, Carlsbad, CA) with *Nhe*I and *Bgl*II and ligated it to the corresponding sites in pGL3 Basic (Promega, Madison, WI). EF-1α and FL were excised with *Nhe*I and *Xba*I and blunt end ligated to the *Pac*I site of the lentiviral vector FUGW (ref. 17; gift of David Baltimore, California Institute of Technology) to produce FUGW-FL. FUGW-FL produces constitutive expression of FL and EGFP from EF-1α and ubiquitin promoters, respectively.

Stocks of FUGW-FL were prepared by transient transfection of 293T cells and were concentrated as described previously (17). 4T1 cells were transduced at a multiplicity of infection (MOI) of 2 in the presence of 8 μg/mL polybrene (Sigma, St. Louis, MO). Transduced 4T1 cells were identified by expression of green fluorescent protein (GFP), and 4T1-GFP-FL cells were sorted by flow cytometry for *in vitro* and *in vivo* experiments.

For RNAi of CXCR4, we expressed short hairpin RNA molecules targeted to sites beginning at nucleotides 5 and 101 in the mouse mRNA. The following oligonucleotides (synthesized by Integrated DNA Technologies, Coralville, IA) were used: (*a*) position 5, 5′-GATCCCGCCGATCGTGTGAGTATATTTCAAGAGAATATACTCACACTGATCGGTTTTTTGGAAA-3′ and 5′-AGCTTTTCCAAAAAACCGATCAGTGTGAGTATATTCTCTTGAAATATACTCACACTGATCGGCGG-3′; and (*b*) position 101, 5′-GATCCCAACGTCCATTTCAATAGGATTCAAGAGATCCTATTGAAATGGACGTTTTTTTTGGAAA-3′ and 5′-AGCTTTTCCAAAAAAAACGTCCATTTCAATAGGATCTCTTGAATCCTATTGAAATGGACGTTGG-3′. Oligonucleotides were annealed and ligated to pSilencer 2.1-U6 hygromycin (Ambion, Austin, TX) according to the manufacturer's directions. This vector contains a human U6 promoter to express short hairpin RNA and a hygromycin selection marker.

4T1-GFP-FL cells were transfected with short hairpin RNA plasmids targeted to either position 5 or 101 with Fugene 6 (Roche, Indianapolis, IN). Stable transfectants were isolated by culture in 250 μg/mL hygromycin (Invitrogen), and transfected RNAi 5 and RNAi 101 cells were passaged in hygromycin approximately every 2 weeks.

Immunoblotting. 80 μg whole cell lysate as determined by BCA analysis (Pierce, Rockford, IL) were loaded per lane for Western blot analysis. CXCR4 and glyceraldehyde-3- phosphate dehydrogenase (GAPDH) proteins were detected as described previously (18), with primary rabbit polyclonal antibodies (Abcam, Cambridge, MA, and Santa Cruz Biotechnology, Santa Cruz, CA, respectively) and a goat antirabbit secondary antibody coupled to horseradish peroxidase (Amersham, Piscataway, NJ).

Immunohistochemistry and Quantification of Tumor Blood Vessels. Resected primary tumors were snap-frozen in Tissue Tek O.C.T. compound (Sankura Finetek, Torrance, CA) and were sectioned at 10-μm intervals. Sections were stained for CD31 antigen with a primary rabbit polyclonal antibody (Santa Cruz Biotechnology) with standard immunohistochemistry techniques. CD31 was detected with a Vectastain ABC kit for peroxidase staining (Vector Laboratories, Burlingame, CA), and sections were counterstained with hematoxylin. Tumor vascularity was quantified by two blinded reviewers (M.S., K.L.) who counted numbers of CD31-stained vessels in 10 randomly selected $\times$40 microscopic fields.

Calcium Assay. Relative changes in intracellular calcium were determined with the cell permeable indicator dye X-rhod-1 (Molecular Probes, Eugene, OR). Approximately 2×10^5 cells were plated in 35-mm glass bottom dishes that were coated with 0.2% gelatin. One day later, cells were washed three times with Modified Earle's Balanced Salt Solution (MEBSS; ref. 19) containing 10% fetal bovine serum and were incubated for 30 minutes in MEBSS containing 1 μmol/L X-rhod-1 and 0.02% Pluronic-F127 (Molecular Probes). Cells again were washed three times with MEBSS and then were incubated for 10 minutes before assay.

Calcium assays were done on a LSM 5 PASCAL system for confocal microscopy coupled to an Axiovert 200 microscope (Zeiss, Thornwood, NY). Images were obtained every 20 seconds with a 40X water immersion objective, with argon 488 and HeNe 543 laser lines for GFP and X-rhod-1, respectively. After collecting baseline images for 2 minutes, cells were treated with 200 ng/mL mouse CXCL12-α (Peprotech, Rocky Hill, NJ) or 20 μmol/L ionomycin (Sigma). In some experiments, cells were treated sequentially with CXCL12-α and ionomycin. Increases in X-rhod-1 fluorescence, which correspond to increased intracellular calcium, were quantified with Zeiss LSM software to define regions-of-interest (ROI) of 10 areas within a field. Data for X-rhod-1 fluorescence were normalized to GFP constitutively expressed by transduced 4T1 cells.

***In vitro* Measurements of Luciferase Activity.** To quantify FL activity, 3.5×10^4 4T1-GFP-FL, RNAi 5, and RNAi 101 cells were plated in 24-well plates. One day later, cells were lysed in reporter lysis buffer (Promega), and bioluminescence from FL was measured on a luminometer (Turner Designs Luminometer Model TD-20/20). FL activity was normalized to milligrams of total cell protein assayed by BCA (Pierce). Parallel assays showed that 15,500 cells contained 0.1 mg of total cell protein.

***In vitro* Cell Proliferation.** One $\times 10^4$ 4T1-GFP-FL, RNAi 5, or RNAi 101 cells per well were seeded in triplicate 6-well plates in 2 mL of growth medium on day 0. Cells were trypsinized, resuspended in a total volume of 1 mL of medium, and counted with a hemacytometer at intervals shown on figure legends.

Animal Studies. Animal handling and procedures were approved by the Washington University School of Medicine Animal Studies Committee. Implantation of 7×10^3 4T1-GFP-FL, RNAi 5, or RNAi 101 cells into the right inguinal mammary gland of 6-to-10-week-old female BALB/c mice (Taconic, Germantown, NY), and surgical resection of the primary tumor 21 days later, were done as described previously (20). The volume of primary tumors was quantified as the product of caliper measurements in three dimensions. Bioluminescence imaging was performed on all of the mice twice a week after tumor implantation, and selected animals were imaged approximately once a week by magnetic resonance imaging (MRI).

To directly produce lung metastases, mice were given injections of 1×10^6 4T1-GFP-FL, RNAi 5, or RNAi 101 cells by tail vein. Bioluminescence imaging was performed on all of the animals at the times indicated in figure legends. For experiments with the CXCR4 antagonist AMD3100 (Sigma), mice were given injections of 1.25 mg/kg AMD3100 or PBS vehicle subcutaneously twice a day beginning 3 hours after tail vein injection of 4T1 cells.

Animals were sacrificed when moribund, and sites of metastases were determined by visual inspection. In selected mice, tumor foci were localized by *ex vivo* luciferase assay or formation of 6-thioguanine-resistant colonies.

Bioluminescence Imaging. Mice were intraperitoneally given injections of 150 μg/g D-luciferin in PBS, and bioluminescence imaging with a charge-coupled device (CCD) camera (IVIS, Xenogen, Alameda, CA) was initiated 10 minutes after injection (21). Bioluminescence images were obtained with a 15-cm field of view (FOV), binning (resolution) factor of 8, 1/f stop, and open filter. Imaging times were 1 to 60 seconds, depending on the amount of luciferase activity. Bioluminescence from ROI was defined manually, and data were expressed as photon flux (photons/s/cm^2/steradian). Background photon flux was defined from a ROI drawn over a mouse that was not given an injectio0n of luciferin.

Magnetic Resonance Imaging. MR images of mice were collected in an Oxford Instruments (Oxford, United Kingdom) 4.7 tesla, 40-cm bore magnet. The magnet is equipped with Magnex Scientific (Oxford, United Kingdom) actively shielded, high-performance (10 cm inner diameter, 60 G/cm, 100 μs rise-time) gradient coils and is interfaced with a Varian NMR Systems (Palo Alto, CA) INOVA console. Data were collected with a Stark Contrast (Erlangen, Germany) 2.5 cm birdcage RF coil. Tumor formation and development in lung and liver were monitored with multislice, coronal, respiratory-gated spin echo MR images as described previously (22). Spin-echo imaging settings were TR = 3 seconds, TE = 20 milliseconds, 5.0 cm FOV, slice thickness = 0.5 mm, 4 scans. During the imaging experiments, the respiration rates for all mice were regular and $\sim$2 s^{-1}, enabling image acquisition during postexpiratory periods.

Uptake and distribution of contrast agent within tumors was monitored with T1-weighted gradient-echo experiments. An intraperitoneal catheter was inserted into each mouse before its being placed into the birdcage coil. Multislice, gradient echo images were collected with TR = 60 ms; TE = 1.6 ms, 2.5-cm FOV, slice thickness = 1 cm; 8 scans. These images required approximately 1 minute to acquire. After the collection of two precontrast images,

150 μL of Omniscan contrast agent (gadodiamide; Amersham Health, Piscataway, NJ), diluted 1:10 in saline, were injected intraperitoneally and additional images were collected for a total of 25 minutes. Tumors were manually segmented, and the average intensity within the tumor was measured as a function of time with Varian's Image Browser software (Varian, Palo Alto, CA). Data for contrast agent uptake were plotted as tumor intensity *versus* time.

Detection of 4T1 Tumor Cells by 6-Thioguanine Resistance. Clonogenic 4T1 tumor cells in whole blood, liver, lung, spleen, brain, lymph nodes, or other tumor sites were detected in selected mice by inherent resistance of 4T1 cells to 60 μmol/L 6-thioguanine (Sigma) as described previously (20).

Statistics. Data are reported as mean values ± SEM and compared with Student's *t* test. Values ≤0.05 were considered significant.

RESULTS

Stable RNA Interference of CXCR4 in 4T1 Breast Cancer Cells. 4T1 cells provide an established model of stage IV breast cancer because these cells form tumors when transplanted into mammary glands of mice and spontaneously metastasize to lungs, liver, lymph nodes, and brain (23). Metastatic cells proliferate with the primary tumor in place and after surgical resection of the primary tumor. 4T1 cells also endogenously express CXCR4 (Fig. 1*A*). To enable noninvasive bioluminescence imaging of primary and metastatic 4T1 cells, we transduced cells with a lentivirus that coexpresses GFP and FL. A population of transduced cells (4T1-GFP-FL) was identified by GFP expression and sorted by flow cytometry (Fig. 1*B*).

To reduce expression of CXCR4 in 4T1-GFP-FL cells, we transiently transfected cells with short hairpin RNA molecules targeted to six different sites in CXCR4 mRNA. RNAi against sequences beginning at positions 5 and 101 of CXCR4 mRNA transiently decreased expression of CXCR4 protein to 30% or less of that detected in parental cells (data not shown). We stably expressed these plasmid-based short hairpin RNAi molecules in 4T1-GFP-FL cells and used immunoblotting to identify clonal cells with reduced expression of CXCR4 protein (Fig. 1*A*). We selected two different cell lines, one each from cells that expressed RNAi constructs to positions 5 or 101, respectively. By densitometry, levels of CXCR4 in each cell line were reduced to ~20% of those present in 4T1-GFP-FL cells. Stably transfected cells, designated RNAi 5 and RNAi 101, respectively, also were sorted by flow cytometry for GFP to use in subsequent experiments. Luciferase activity in cell lysates was equivalent for 4T1-GFP-FL and RNAi 101 cells, whereas RNAi 5 cells had lower luciferase activity than the other two cell types (Fig. 1*C*).

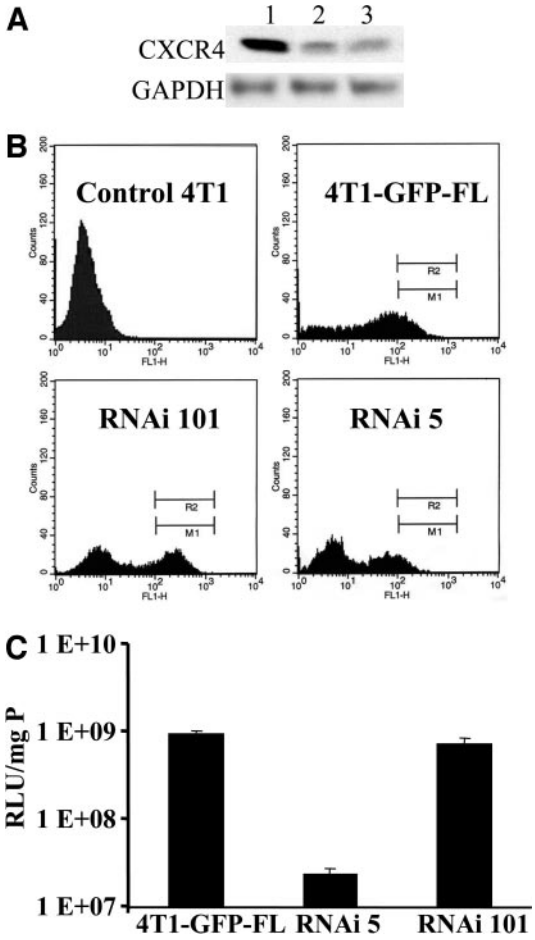

Fig. 1. Stable RNAi of transduced 4T1 breast cancer cells. *A*, Western blot for CXCR4 protein (*top panel*) in 80 μg of whole cell lysates of 4T1-GFP-FL (*Lane 1*), RNAi101 (*Lane 2*), and RNAi5 (*Lane 3*) cells. Levels of GAPDH (*bottom panel*) are shown as a loading control. In *B*, 4T1 cells were transduced with a lentivirus expressing GFP and FL and were sorted by flow cytometry for expression of GFP (4T1-GFP-FL cells). Cells, stably transfected with short hairpin RNA molecules to sequences beginning at base 5 (RNAi 5) or 101 (RNAi 101 cells), also were sorted for GFP expression. Gates define populations of sorted cells (*R2*, *M 1*), and untransduced 4T1 cells are shown as a negative control (*Control 4T1*). *C*, *in vitro* luciferase activity. Cells were plated at a density of 3.5×10^4 cells per well in 24-well plates. One day later, luciferase activity in cell lysates was quantified on a luminometer. Data are presented as mean values ± SEM for relative light units per milligram of protein (*RLU/mg P*; $n = 4$). Data are representative of two independent experiments.

CXCL12 binding to CXCR4 produces transient increases in intracellular calcium. To determine whether reduced expression levels of CXCR4 functionally inactivated signaling, we analyzed levels of intracellular calcium in response to treatment with CXCL12. In parental 4T1-GFP-FL cells, incubation with 200 ng/mL CXCL12 produced the expected rapid increase in intracellular calcium (24), as quantified with the calcium-sensitive dye X-rhod-1 (Fig. 2*A*). By comparison, no change in intracellular calcium was detected in RNAi 5 and RNAi 101 cells treated with the same concentration of CXCL12. As a positive control, we treated cells with 20 μmol/L ionomycin, a calcium ionophore. Incubation with ionomycin increased intracellular calcium in all cells, although the relative change was slightly lower in RNAi 5 cells compared with parental 4T1-GFP-FL and RNAi 101 cells. Potentially, this difference may be due to clonal variations or off-target effects of RNAi 5. Overall, these data show that knockdown of CXCR4 with two different RNAi constructs inhibits response to CXCL12.

CXCR4 has been shown to directly or indirectly regulate proliferation of some breast cancer cell lines in culture (25). To establish if decreased expression of CXCR4 affected proliferation of 4T1 cells *in vitro*, we quantified cell growth over a 4-day interval after plating cells at low density in standard culture medium (Fig. 2*C*). Proliferation of 4T1-GFP-FL, RNAi 5, and RNAi 101 cells did not differ significantly ($P > 0.6$), demonstrating that expression levels of CXCR4 did not affect cell growth under normal culture conditions.

Reduced Expression of CXCR4 Inhibits Growth of Orthotopic 4T1 Tumors. To investigate whether reduced CXCR4 expression and signaling affected progression of primary and metastatic breast cancer, we injected 7×10^3 4T1-GFP-FL, RNAi 5, or RNAi 101 cells into inguinal mammary fat pads of BALB/c mice. We performed RNAi bioluminescence imaging (BLI) studies of each mouse twice a week and used the well-established correlation between *in vivo* bioluminescence and tumor size at a given site as one measure of primary tumor growth (26). Over a period of 17 days, photon flux from 4T1-GFP-FL cells at the primary tumor site increased more rapidly than did either RNAi 5 or RNAi 101 cells (Fig. 3*A* and *B*). Differences between RNAi cell lines and parental 4T1-GFP-FL were significant ($P < 0.05$ or $P < 0.005$, respectively) at all time points except day 14 for RNAi 101 cells. Because 4T1-GFP-FL and RNAi 101 cells have

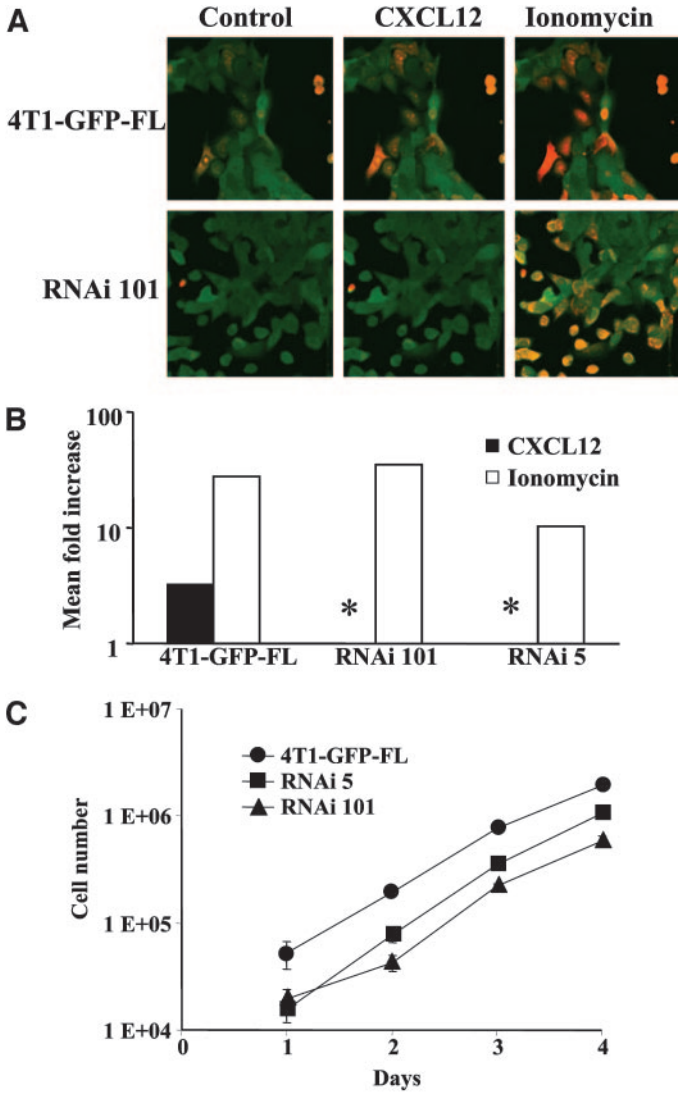

Fig. 2. *In vitro* characterization of 4T1-GFP-FL and cells with RNAi against CXCR4. *A*. CXCL12-mediated intracellular calcium flux. Cells were loaded with the intracellular calcium indicator X-rhod-1 and were treated with 200 ng/mL mouse CXCL12-α or 20 μmol/L ionomycin. Confocal microscope images show X-rhod-1 fluorescence superimposed on GFP in 4T1-GFP-FL and RNAi 101 cells under baseline conditions and 20 seconds after adding CXCL12 or ionomycin. In *B*, time-dependent increases in X-rhod-1 fluorescence were normalized to GFP in each cell line. Fold increases in intracellular calcium 20 seconds after adding CXCL12-α or ionomycin are shown ($n = 3$). *Error bars*, SEM; data are representative of two independent experiments. *, absent response of RNAi 101 and 5 cells to CXCL12-α. *C*, cell proliferation. 4T1-GFP-FL, RNAi 5, and RNAi 101 cells were plated at 1×10^4 cells per well in 6-well plates and were cultured in normal growth medium. Cells were trypsinized and counted to quantify cell proliferation. Data are presented as mean values for cell number ($n = 3$) $\pm$ SEM and are representative of two independent experiments. No significant differences in growth among the three cell lines were observed ($P > 0.6$).

comparable luciferase activities, these data demonstrate that knockdown of CXCR4 substantially inhibited the growth of primary tumors. RNAi 5 cells have lower amounts of luciferase activity than do 4T1-GFP-FL and RNAi 101 cells *in vitro*, accounting for the decreased sensitivity for detecting these cells with BLI. Compared with 4T1-GFP-FL cells, bioluminescence from RNAi 5 tumors is decreased to a greater extent than *in vitro* differences in luciferase activity, and growth rates of RNAi 5 tumors also were relatively slower. Therefore, these data indicate that the inhibition of CXCR4 also reduced growth of RNAi 5 tumors.

To further analyze progression of primary tumors, we measured tumor sizes with calipers 17 days after the implantation of cells, a time at which all of the 4T1-GFP-FL cells had formed palpable tumors. The calculated volume of parental 4T1-GFP-FL cells was significantly greater than that of RNAi 5 and RNAi 101 cells ($P < 0.001$; Fig. 3*C*). Differences in tumor volume between control and RNAi cells were proportionately greater than were differences in luciferase activity measured by BLI. This disparity likely is due to the different conditions measured with each technique. Only viable cells produce luciferase activity (BLI), whereas necrotic and viable tissue both contribute to tumor volume. Before surgical resection (day 21), many of the control 4T1-GFP-FL tumors developed areas of ulceration. Areas of ulceration are included in 4T1-GFP-FL tumor volumes but do not produce bioluminescence. By comparison, RNAi tumors did not have ulceration, so a smaller measured volume of tumor cells will

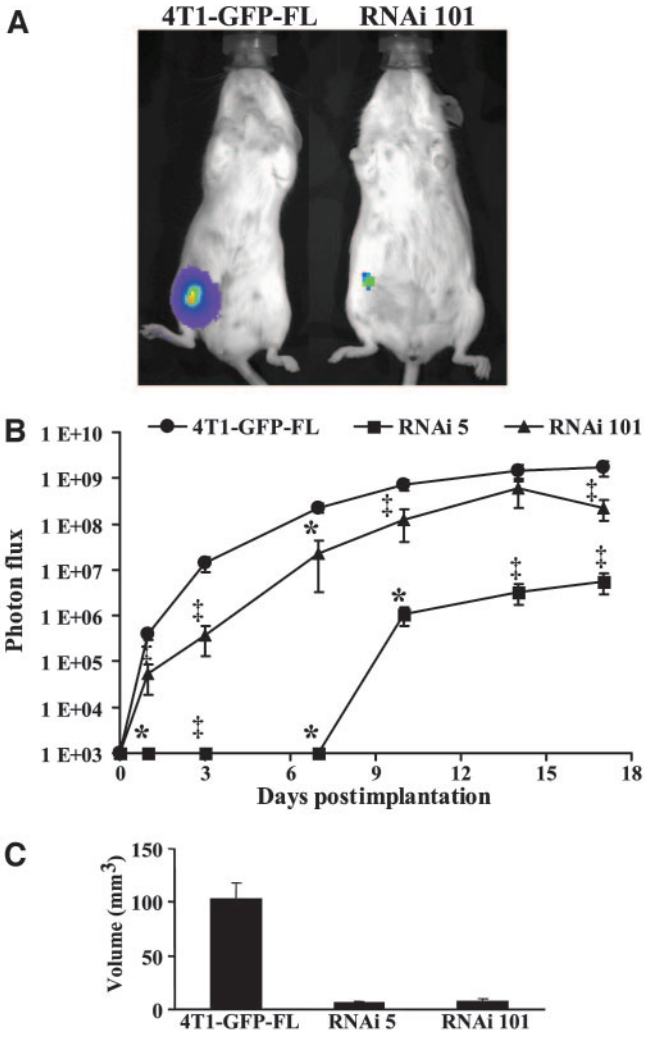

Fig. 3. Effects of reduced CXCR4 on primary breast tumors. Seven $\times 10^3$ 4T1-GFP-FL, RNAi 5, and RNAi 101 cells were implanted into right inguinal mammary fat pads of BALB/c mice. *A*, representative BLI images of primary 4T1-GFP-FL and RNAi 101 breast tumors 3 days after implantation. Mice were given injections of 150 mg/kg luciferin intraperitoneally and were imaged on the CCD camera 10 minutes after injection. BLI images were collected for 1 or 10 seconds for 4T1-GFP-FL and RNAi 101 cells, respectively. Different image acquisition times were needed to avoid saturating the CCD camera. Bioluminescence is presented as a pseudocolor scale: *red*, the highest photon flux; *blue*, the lowest photon flux. In *B*, bioluminescence from primary tumors was quantified by ROI analysis of images obtained on the indicated days (*horizontal axis*) after cell implantation. Increases in bioluminescence correlate directly with greater number of cells. Background bioluminescence was subtracted from each tumor ROI value; data represent mean values $\pm$ SEM for photon flux in each group ($n = 8$). The *ordinate of the graph*, log scale. *, statistically significant difference ($P < 0.005$); ‡, statistically significant difference ($P < 0.05$). In *C*, tumor sizes in three dimensions were measured by calipers 17 days after implantation of cancer cells; data are presented as mean $\pm$ SEM for tumor volume ($n = 8$ for each cell type).

produce relatively greater bioluminescence because all of the cells are viable. Overall, the combination of BLI data and tumor volumes demonstrate that knockdown of CXCR4 substantially limits the growth of orthotopic primary 4T1 breast cancer cells.

One possible mechanism for more rapid growth of 4T1-GFP-FL tumors is enhanced angiogenesis. CXCL12 signaling through CXCR4 stimulates the production of vascular endothelial growth factor (VEGF; ref. 27), and VEGF also has been demonstrated to up-regulate CXCR4 in breast cancer cells (4). Knockdown of CXCR4 potentially could disrupt this autocrine-positive feedback loop in RNAi tumors. To noninvasively investigate steady-state perfusion and permeability of primary tumors, we used MRI with the blood-pool contrast agent gadodiamide to study four mice each with 4T1-GFP-FL and with RNAi 101 tumors. After intraperitoneal injection of gadodiamide, sequential images of primary tumors were obtained over 25 minutes, and changes in signal intensity within tumors were normalized to baseline images without contrast (Fig. 4*A* and *B*). Time-dependent increases in signal were comparable in both tumor types, indicating that steady-state delivery and retention of the vascular contrast agent was not affected by CXCR4 levels in 4T1-GFP-FL and RNAi 101 cells.

We also analyzed vascularity by immunohistochemistry in excised tumors from 4T1-GFP-FL, RNAi 5, and RNAi 101 cells. Tumor blood vessels were defined by the endothelial-cell marker CD31, and two blinded reviewers (M.S., K.L.) quantified the numbers of vessels in 10 randomly selected microscopic fields (Fig. 4*C* and *D*). Intratumoral vessels did not differ between 4T1-GFP-FL and RNAi 101 tumors, which confirmed MRI data for tumor perfusion. By comparison, RNAi specimens had a small but significant ($P < 0.05$) reduction in blood vessels, which could contribute to the decreased growth of RNAi 5 primary tumors. Because angiogenesis was not affected by both RNAi constructs, it is likely that decreased numbers of blood vessels in RNAi 5 tumors are due to clonal variations rather than to effects of CXCR4 inhibition on angiogenesis.

Knockdown of CXCR4 Prevents Macroscopic Metastases of 4T1 Cells. 4T1 breast cancer cells spontaneously form metastases, independent of primary tumor resection (28). Surgical resection of primary tumors reproduces clinical treatment of patients with breast cancer. In our model system, the removal of large primary tumors improves the sensitivity of BLI for detecting metastases because high amounts of luciferase activity in these tumors potentially could obscure small metastatic tumors. We resected primary tumors in all eight of the mice into which 4T1-GFP-FL cells were implanted, and we resected the four largest tumors each in mice into which RNAi 5 and RNAi 101 cells, respectively, were implanted. In the remaining mice that received RNAi cells, primary tumors were <3 mm in diameter and, therefore, were not removed.

We used BLI and MRI to detect and monitor breast cancer metastases in the mice described above that had received implants of 4T1-GFP-FL, RNAi 5, and RNAi 101 cells. All eight mice with 4T1-GFP-FL tumors developed tumor metastases with lung as the predominant organ (Fig. 5). These mice all died as a result of metastatic breast cancer within 56 days of tumor implantation. Sites of macroscopic metastases identified with noninvasive imaging were confirmed in selected mice by the *ex vivo* imaging of luciferase activity or the isolation of 4T1 cells from tissues based on 6-thioguanine resistance (data not shown). In all of the mice, macroscopic metastases were confirmed by dissection and visual inspection at autopsy (Fig. 5*C*).

Remarkably, no mouse that received an implant of either RNAi 5 or RNAi 101 cells had macroscopic metastases detectable with noninvasive imaging. This result likely is due to the substantially impaired growth of the primary tumors from both of the RNAi cell lines. In the

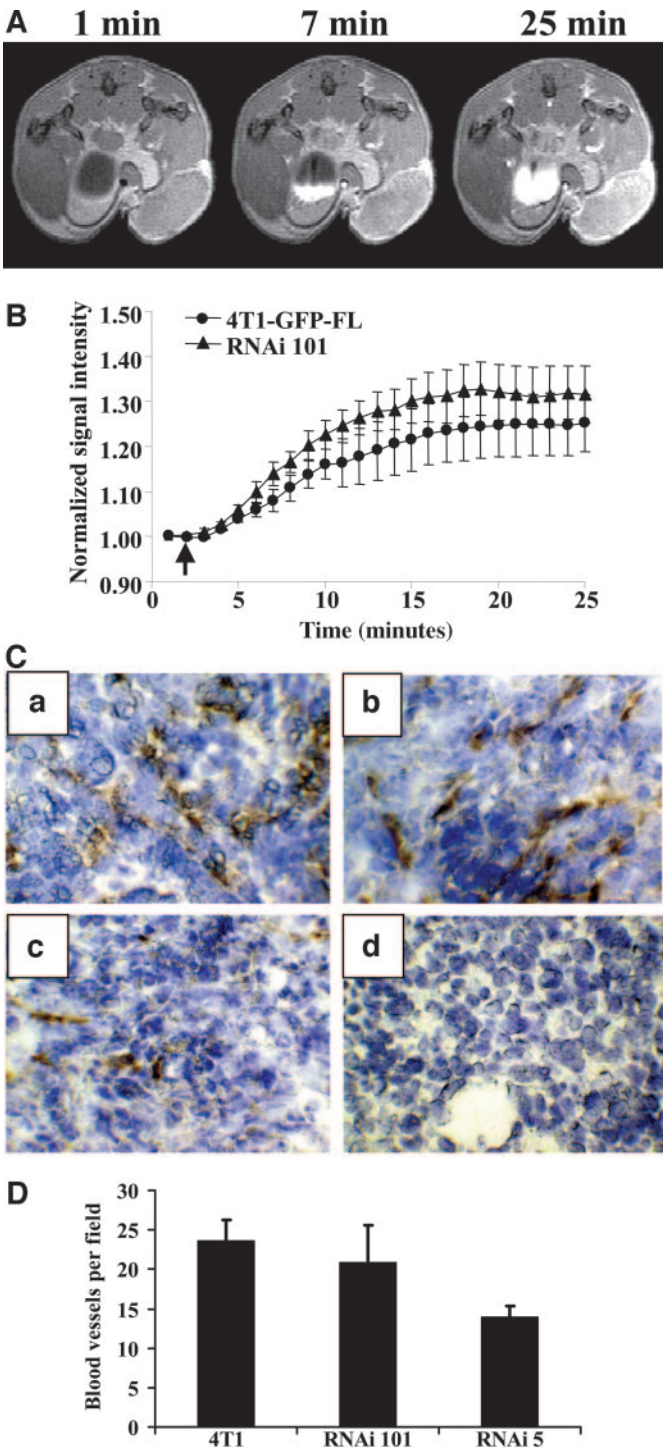

Fig. 4. Effects of reduced CXCR4 on tumor angiogenesis. In *A*, steady-state contrast enhancement is comparable in 4T1-GFP-FL and RNAi 101 tumors. Sequential T1-weighted gradient-echo images were acquired at 1-minute intervals (*1 min*) in mice in which 4T1-GFP-FL or RNAi 101 cells ($n = 4$ each) were implanted. Gadodiamide (150 μL diluted 1:10) was infused intraperitoneally during acquisition of the 2-minute image. Representative images are shown from a mouse with 4T1-GFP-FL tumors at times 1, 7, and 25 minutes (*1 min, 7 min, 20 min*) after the start of imaging. The 1-minute image is acquired before infusion of contrast. *B*, calculated increases in tumor signal intensity after contrast administration. Signal intensity was measured by ROI analysis and was normalized to baseline tumor signal without contrast material. Data are mean values ± SEM ($n = 4$). *Arrow*, the start of contrast infusion. *C*, immunohistochemistry staining (*brown*) of the endothelial marker CD31 in primary tumors. Representative sections (×40) are shown from 4T1-GFP-FL (*a*), RNAi 101 (*b*), and RNAi 5 (*c*) tumors. No staining is seen in the control 4T1-GFP-FL tumor incubated with secondary antibody alone (*d*). *D*, mean number of blood vessels per ×40 microscopic field. CD31-stained blood vessels were quantified in 10 randomly selected areas of tumor specimens. Data are mean values + SEM. Differences between 4T1-GFP-FL and RNAi 101 cells were not significantly different ($P > 0.7$), but fewer blood vessels were detected in RNAi 5 tumors ($P < 0.05$).

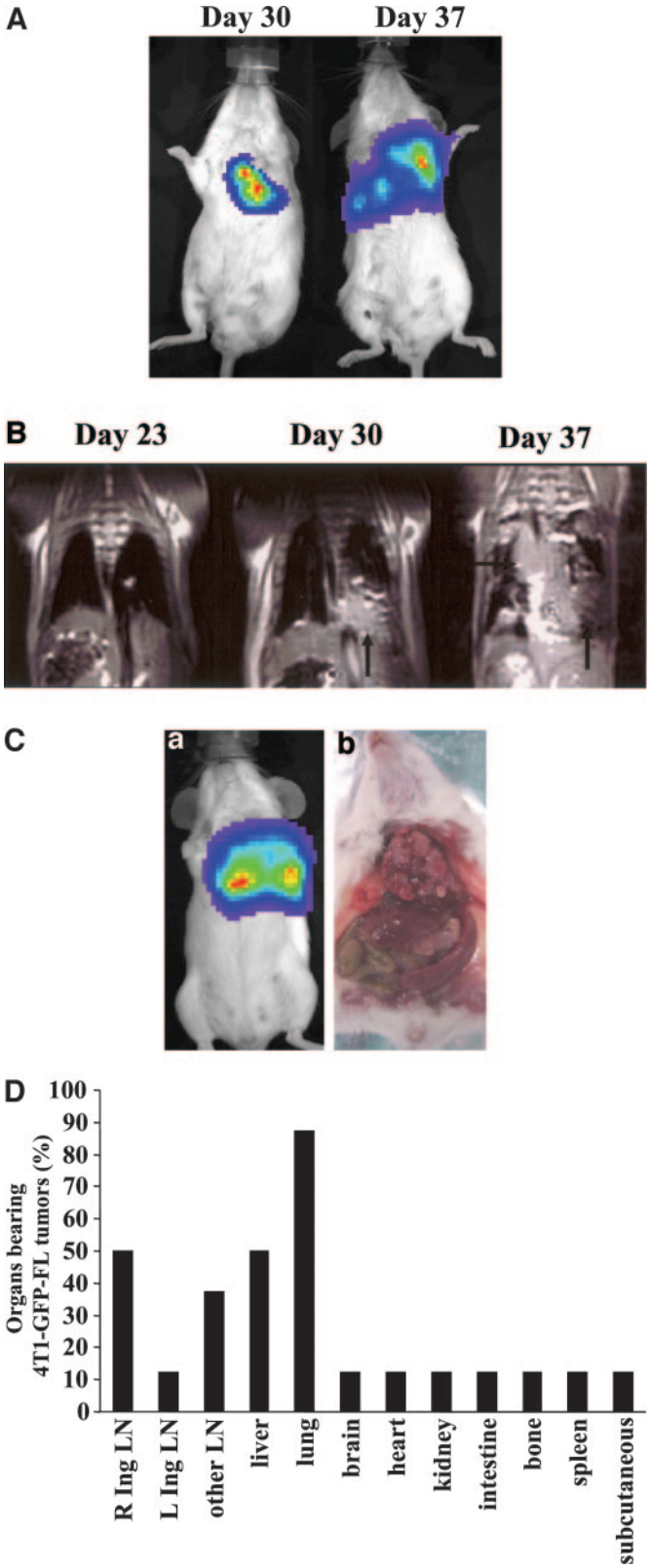

Fig. 5. Spontaneous metastases occur only from orthotopically injected 4T1-GFP-FL tumors. Progression of breast cancer metastases was detected and monitored with noninvasive BLI and MRI. In *A*, 1-minute BLI images obtained 30 and 37 days after implantation of 4T1-GFP-FL cells show progression of lung metastases. In *B*, representative coronal T1-weighted images of the same mouse show anatomic localization and size of lung metastases produced by 4T1-GFP-FL cells. No lung tumors were detected on day 23 postimplantation, whereas subsequent images show rapid progression of lung metastases and replacement of normal lung tissue (*arrows*). In *C*, bioluminescence image (*a*) obtained 1 day before death shows diffuse lung metastases, corresponding to the findings at autopsy (*b*). *D*, distribution of metastases in various anatomic sites in mice implanted with 4T1-GFP-FL cells. Metastases were identified in living mice with noninvasive BLI and MRI and were confirmed by autopsy. For selected mice, metastases also were verified by *ex vivo* imaging of luciferase activity or culture of 6-thioguanine-resistant 4T1-GFP-FL cells from organs and tissues. Data are shown as the percentage of mice ($n = 8$) with metastases at the listed sites. No metastases were identified in mice in which RNAi 5 or RNAi 101 cells were implanted. *R Ing LN*, right inguinal lymph node; *L Ing LN*, left inguinal lymph node; *other LN*, axillary, mediastinal, and mesenteric lymph nodes.

four mice from each group that did not have resection of primary tumor, the primary tumor regressed and became undetectable by BLI or palpation within 30 days of cell implantation. All of these mice were alive and healthy 90 days after tumor implantation, which greatly exceeded the survival of mice in three different experiments with parental 4T1-GFP-FL cells (data not shown). These data show that the knockdown of CXCR4 with stable RNAi prevents the development of macroscopic 4T1 cell metastases in this mouse model of metastatic breast cancer. Furthermore, these data suggest that CXCR4 signaling may be necessary for continued survival of breast cancer cells in the primary tumor site.

RNA Interference or Pharmacological Inhibition of CXCR4 Delays Initial Growth of Experimental Lung Metastases. Because RNAi of CXCR4 prevented macroscopic metastases of 4T1 cells from the mammary fat pad, we could not assess the effects of CXCR4 on tumor growth in other organs. We injected 1×10^6 4T1-GFP-FL, RNAi 5, or RNAi 101 cells by tail vein to directly introduce cancer cells to lung, an organ with high levels of CXCL12 (3) and the most common site of metastases from orthotopically placed 4T1-GFP-FL tumors. Mice were imaged over 7 days after the injection, and data for luciferase activity in lung were normalized to initial bioluminescence at 3 hours to account for differences in injection of tumor cells and lower luciferase activity in RNAi 5 cells (29).

ROI analysis of lungs showed an immediate decrease in bioluminescence between 3 and 16 hours for all cells, with luciferase activity at 16 hours being approximately 20% of that at the initial 3-hour time point (Fig. 6). Decreases in cell number were comparable for both cell lines, indicating that the initial inefficiency of the metastatic process in lung was not affected by levels of CXCR4 (30, 31). As measured by ROI analysis of BLI images, normalized photon flux from 4T1-GFP-FL cells progressively increased through 1 week, reaching levels more that 11-fold greater than the initial lung value at 3 hours. By comparison, normalized luciferase activity from RNAi 5 and 101 cells in lung was significantly lower than that from 4T1-GFP-FL cells at all times after 24 hours, indicating that proliferation and/or survival of RNAi cells was inhibited significantly ($P < 0.05$). These early differences in growth or survival of breast cancer cells in lung could be mediated by the mitogenic and/or antiapoptotic effects of CXCR4, respectively (14, 25, 32).

We could not perform BLI for more than 7 days after cell injection because luciferase activity from 4T1-GFP-FL cells exceeded detection limits of the CCD camera, so that bioluminescence data were no longer quantitatively accurate. We continued to monitor the animals until they were moribund from tumor burden. Despite the initial growth lag for RNAi 5 and 101 cells in lung, mice that received injections of RNAi cells did not survive longer than animals with parental 4T1-GFP-FL cells. All of the animals became moribund between days 16 and 18 after the injection of cells.

As an alternative to RNAi, we treated mice with AMD3100, a specific inhibitor of CXCR4 (16) that has been shown recently to inhibit growth of intracranial brain tumor xenografts in mice (14). Mice were given injections via tail vein with 1×10^6 4T1-GFP-FL cells and were imaged with BLI 3 hours later to establish a baseline for luciferase activity. Animals then were treated twice a day with 1.25 mg/kg AMD3100 or PBS, injected subcutaneously (14). Similar

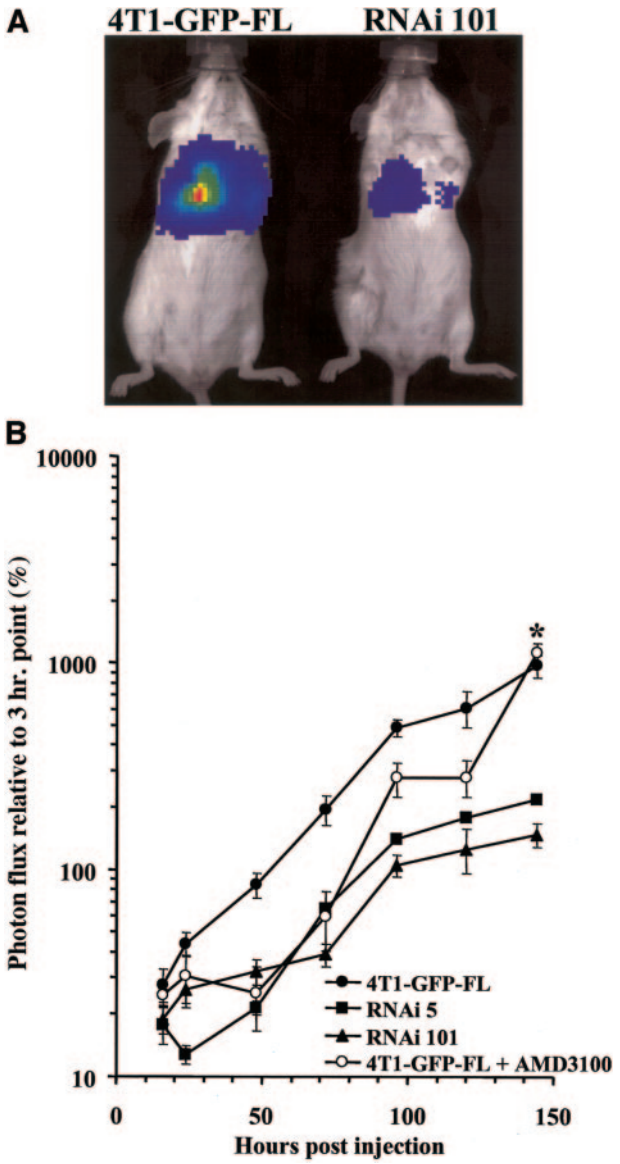

Fig. 6. Inhibition of CXCR4 delays growth of experimental 4T1 lung metastases. In *A*, 1×10^6 4T1-GFP-FL, RNAi 5, or RNAi 101 cells were injected via tail vein to produce lung metastases. Mice injected with 4T1-GFP-FL cells were treated with twice daily subcutaneous doses of 1.25 mg/kg AMD3100 or PBS beginning 3 hours after intravenous injection. Mice with RNAi 5 or 101 tumors received PBS control. Representative BLI images of lung metastases in PBS-treated mice injected with 4T1-GFP-FL or RNAi 101 cells at 48 hours. In *B*, ROI analysis of BLI images was used to quantify changes in cell number over time. Data for photon flux were normalized to bioluminescence at 3 hours to account for initial differences in numbers of cells reaching lung. Data are mean values ± SEM from two independent experiments for parental and RNAi cell lines (n = 10–12 mice per group) and one experiment with AMD3100 (n = 6 mice). All values for RNAi- and AMD3100-treated cells are statistically different from parental 4T1-GFP-FL cells after 24 hours ($P < 0.05$) except for AMD3100 at 144 hours (*). Values at 16 and 24 hours were not significantly different. *Ordinate*, log scale.

to data with RNAi 101 cells, the inhibition of CXCR4 with AMD3100 significantly decreased numbers of 4T1-GFP-FL cells in lung after 24 hours, as determined by BLI ($P < 0.05$; Fig. 6*B*). The lag in cell proliferation and/or survival produced by AMD3100 was less than that observed in RNAi cells, likely because intermittent dosing of AMD3100 was less effective than RNAi in blocking CXCR4 signaling. After 7 days, cells in mice treated with AMD3100 had overcome the initial delay in proliferation, showing normalized bioluminescence that did not differ from that of 4T1-GFP-FL cells in mice receiving PBS vehicle control. Similar to results with RNAi cells, AMD3100 treatment of mice with 4T1-GFP-FL cells did not prolong survival relative to vehicle control. These data with RNAi and pharmacological blockade of CXCR4 indicate that this chemokine receptor substantially enhances the initial growth of breast cancer cells in lung, although interrupting the CXCR4 signaling alone is not sufficient to prolong overall survival.

DISCUSSION

Chemokines and chemokine receptors recently have been proposed to have important functions in breast cancer (3, 33, 34). In particular, CXCL12-mediated signaling through CXCR4 in breast cancer cells may regulate organ-specific trafficking and invasion of metastatic tumor cells. Common sites of breast cancer metastases, including lung, liver, lymph node, and bone, express high levels of CXCL12 (3), and gradients of this chemokine are hypothesized to account for tissue tropism of breast cancer metastases. In models of metastatic breast cancer with immunodeficient mice, the administration of neutralizing antibodies or peptide antagonists of CXCR4 substantially reduce lung metastases (3, 8, 35). CXCR4 expression is up-regulated in murine lung metastases in a nuclear factor-κB–dependent fashion (10), again suggesting that CXCR4 signaling is an important determinant of metastatic breast cancer. Furthermore, humans with invasive ductal breast carcinoma show a significant correlation between relative expression levels of CXCR4 and the extent of lymph node metastases (36).

Whereas previous studies suggest that CXCR4 regulates breast cancer metastases, our current data extend these observations by demonstrating that CXCR4 has substantial functions in both primary and metastatic breast cancer in immunocompetent mice. We used stable RNAi directed against two different sites in CXCR4 mRNA to knockdown expression of CXCR4 and CXCL12-mediated signal transduction in murine 4T1 cells. After orthotopic implantation into mammary fat pads, parental 4T1-GFP-FL cells with endogenous expression of CXCR4 grew more rapidly than RNAi knockdown cells. In addition to delayed growth of RNAi cells in primary tumors, some of these tumors regressed after approximately 2 weeks. These data suggest that CXCR4 is necessary for proliferation and survival of breast cancer cells in the primary tumor site. This result contrasts with cell growth under standard culture conditions, in which levels of CXCR4 did not affect proliferation rates. These data indicate that CXCR4 is essential for cell growth under conditions in which survival and growth factors are limiting, such as the *in vivo* tumor microenvironment. Similar positive effects of CXCR4 on cell growth have been reported for an ovarian cancer cell line cultured under suboptimal conditions *in vitro* (37).

Our results are consistent with a recent study of human breast cancer that also demonstrates the importance of the primary tumor microenvironment in CXCL12-CXCR4 signaling (7). Expression of CXCR4 was increased in invasive ductal carcinoma specimens compared with ductal carcinoma *in situ* and normal breast epithelium, and CXCL12 was overexpressed by normal breast stromal cells adjacent to malignant cells. The authors [Allinen et al. (7)] proposed that CXCL12 in the tumor microenvironment functioned to promote breast cancer proliferation, migration, and invasion. RNAi against CXCR4 in breast cancer cells could interrupt this paracrine signaling pathway, potentially accounting for the impaired growth and survival of primary tumors observed in our study.

All of the mice into which parental 4T1 cells were implanted developed palpable tumors within 3 weeks and, subsequently, had spontaneous breast cancer metastases that most commonly affected lung. All mice into which parental 4T1 cells were implanted died within 60 days. Animals with RNAi cells survived through 90 days without evidence of metastases, likely because of the limited growth

of primary tumors. The inhibition of primary breast tumor growth and spontaneous metastases were comparable with both of the stable RNAi molecules, providing strong evidence that effects were specific to CXCR4 and not due to variations in cell lines or off-target results of RNAi. Overall, these data show that the *in vivo* proliferation of 4T1 cells in the primary tumor site and the development of macroscopic metastases are both highly dependent on expression levels of CXCR4.

CXCL12-CXCR4 activates numerous signaling pathways in breast cancer cells *in vitro* (38), so that there are many potential mechanisms through which CXCR4 could affect both primary and metastatic breast cancer. Because expression of CXCR4 and VEGF can provide a positive feedback loop and because angiogenesis is essential for tumor growth and metastases (reviewed in ref. 39), we initially investigated whether primary tumor vasculature contributed to *in vivo* differences between parental and RNAi 4T1 cells. MRI and immunohistochemistry showed comparable accumulation of an intravascular contrast agent and numbers of tumor blood vessels, respectively, in parental and RNAi 101 tumors, whereas RNAi 5 tumors had somewhat diminished vascularity. Because effects on vascularity were not concordant between RNAi 5 and 101 tumors, differences likely were due to clonal variations and were not specifically caused by blocking CXCR4 signaling in breast cancer cells. Further investigation is needed to dissect how other downstream effectors of CXCR4, such as AKT and extracellular signal-regulated kinases 1 and 2 (Erk 1 and 2), regulate primary breast cancer proliferation, survival, and invasion.

To investigate the effects of CXCR4 on breast cancer growth in a metastatic site, we produced experimental lung metastases with parental and RNAi cells and used noninvasive BLI to measure temporal changes in cell number. After intravenous injection, all of the cells had comparable decreases in bioluminescence, indicating that reduced expression of CXCR4 did not affect initial metastatic inefficiency. Compared with parental 4T1 cells, growth of RNAi 5 and 101 lung metastases was delayed substantially, showing that reduced CXCR4 correlated with a marked reduction in cell proliferation and/or survival. A similar function for CXCR4 signaling in growth of experimental colon cancer metastases in lung has been observed recently (9). Using an "intrakine" to decrease plasma membrane expression of CXCR4, Zeelenberg *et al.* showed that CXCR4-deficient cells survived in lungs but did not proliferate, whereas numbers of control cells proliferated rapidly after up-regulating expression of CXCR4 (9). The delay in cell proliferation likely is due to increased apoptosis and/or delayed cell cycle entry in cells with reduced CXCR4. These effects may be mediated by reduced activation of AKT or Erk 1 and 2, pathways that have been correlated with CXCR4–mediated cell proliferation and survival *in vivo* (14). Dissecting how specific CXCR4-regulated signaling pathways contribute to multiple steps in the progression of primary and metastatic breast cancer will further our understanding of CXCR4 in breast cancer, and it is an important area of future research.

As a potential therapeutic model, we used the specific CXCR4 antagonist AMD3100 (16) to treat mice with experimentally produced 4T1-GFP-FL lung metastases. Inhibition of CXCR4 with AMD3100 delayed the initial growth of 4T1-GFP-FL cells in lung compared with the growth in mice that received vehicle control. The early temporal lag in growth was similar to that produced by stable RNAi of CXCR4, although effects of AMD3100 were quantitatively lower and less sustained. This difference likely is due to the persistent inhibition of CXCR4 expression with RNAi compared with the variable antagonism of CXCR4 produced by the rapid decrease in plasma levels of the compound after intermittent subcutaneous dosing (40).

Neither RNAi nor AMD3100 prolonged the survival of mice with experimental lung metastases compared with parental cells treated with vehicle alone. Incomplete effects of CXCR4 inhibition in breast cancer have been reported previously with a peptide antagonist of CXCR4, which produced only a small reduction in experimental lung metastases (35). Potentially, this could be due to the selection of variant cells that are not dependent on CXCR4. Alternatively, CXCR4 may be needed only for the initial growth of lung metastases. These data imply that combination therapy with a CXCR4 inhibitor and other chemotherapeutic drugs may be needed for potential clinical benefits in breast cancer patients.

In summary, we have shown that reduced expression of CXCR4 limits orthotopic growth of breast cancer cells *in vivo* and prevents development of macroscopically detectable metastases from primary tumors. These results extend potential therapeutic applications of CXCR4 inhibitors to the treatment of both primary and metastatic breast cancer. Our model system also demonstrates the advantages of noninvasive imaging techniques to monitor the progression of breast cancer in the same cohort of mice. As new antagonists of CXCR4 become available, *in vivo* imaging techniques will be important tools for determining the therapeutic efficacy of candidate inhibitors and for analyzing how CXCR4 regulates the development and progression of primary and metastatic breast cancer.

REFERENCES

1. Baselga J, Norton L. Focus on breast cancer. Cancer Cell 2002;1:319–22.
2. Liotta L. An attractive force in metastases. Nature (Lond) 2001;410:24–5.
3. Muller A, Homey B, Soto H, et al. Involvement of chemokine receptors in breast cancer metastasis. Nature (Lond) 2001;410:50–6.
4. Bachelder R, Wendt M, Mercurio A. Vascular endothelial growth factor promotes breast carcinoma invasion in an autocrine manner by regulating the chemokine receptor CXCR4. Cancer Res 2002;62:7203–6.
5. Schneider G, Salcedo R, Dong H, Kleinman H, Oppenheim J, Howard O. Suradista NSC 651016 inhibits the angiogenic activity of CXCL12-stromal cell-derived factor 1alpha. Clin Cancer Res 2002;8:3955–60.
6. Schmid B, Rudas M, Resniczek G, Leodoleter S, Zeillinger R. CXCR4 is expressed in ductal carcinoma in situ of the breast and in atypical ductal hyperplasia. Breast Cancer Res. Treat 2004;84:247–50.
7. Allinen M, Beroukhim R, Cai L et al. Molecular characterization of the tumor microenvironment in breast cancer. Cancer Cell 2004;6:17–32.
8. Liang Z, Wu T, Lou H, et al. Inhibition of breast cancer metastasis by selective synthetic polypeptide against CXCR4. Cancer Res 2004;64:4302–8.
9. Zeelenberg I, Ruuls-Van Stalle L, Roos E. The chemokine receptor CXCR4 is required for outgrowth of colon carcinoma micrometastases. Cancer Res 2003;63:3833–9.
10. Helbig G, Christopherson Kn, Bhat-Nakshatri P, et al. NF-kappaB promotes breast cancer cell migration and metastasis by inducing the expression of the chemokine receptor CXCR4. J Biol Chem 2003;278:21631–8.
11. Kang Y, Siegel P, Shu W, et al. A multigenic program mediating breast cancer metastasis to bone. Cancer Cell 2003;3:537–49.
12. Zou W, Machelon V, Coulomb-L'Hermin A, et al. Stromal-derived factor-1 in human tumors recruits and alters the function of plasmacytoid precursor dendritic cells. Nat Med 2001;7:1339–46.
13. Kayali A, Van Gunst K, Campbell I, et al. The stromal cell-derived factor-1alpha/CXCR4 ligand-receptor axis is critical for progenitor survival and migration in the pancreas. J Cell Biol 2003;163:859–69.
14. Rubin J, Kung A, Klein R, et al. A small-molecule antagonist of CXCR4 inhibits intracranial growth of primary brain tumors. Proc Natl Acad Sci USA 2003;100:13513–8.
15. Pulaski B, Terman D, Khan S, Muller E, Ostrand-Rosenberg S. Cooperativity of Staphylococcal aureus enterotoxin B superantigen, major histocompatibility complex class II, and CD80 for immunotherapy of advanced spontaneous metastases in a clinically relevant postoperative mouse breast cancer model. Cancer Res 2000;60:2710–5.
16. De Clercq E. The bicyclam AMD3100 story. Nat Rev Drug Discov 2003;2:581–7.
17. Lois C, Hong E, Pease S, Brown E, Baltimore D. Germline transmission and tissue-specific expression of transgenes delivered by lentiviral vectors. Science (Wash DC) 2002;295:868–72.
18. Luker K, Pica C, Schreiber R, Piwnica-Worms D. Overexpression of IRF9 confers resistance to antimicrotubule agents in breast cancer cells. Cancer Res 2001;61:6540–7.
19. Luker G, Rao V, Crankshaw C, Dahlheimer J, Piwnica-Worms D. Characterization of phosphine complexes of technetium(III) as transport substrates of the multidrug resistance P-glycoprotein and functional markers of P-glycoprotein at the blood-brain barrier. Biochemistry 1997;36:14218–27.
20. Pulaski BA, Ostrand-Rosenberg S. Mouse 4T1 breast tumor model. In: Coligan JE, Kruisbeek AM, Margulies DH, et al, editors. Current protocols in immunology. New York: John Wiley and Sons, Inc; 2003. p.20.2.1
21. Luker G, Bardill J, Prior J, Pica C, Piwnica-Worms D, Leib D. Noninvasive bioluminescence imaging of herpes simplex virus type 1 infection and therapy in living mice. J Virol 2002;76:12149–61.

22. Garbow J, Zhang Z, You M. Detection of primary lung tumors in rodents by magnetic resonance imaging. Cancer Res 2004;64:2740–2.
23. Aslakson C, Miller F. Selective events in the metastatic process defined by analysis of the sequential dissemination of subpopulations of a mouse mammary tumor. Cancer Res 1992;52:1399–1405.
24. D'Apuzzo M, Rolink A, Loetscher M, et al. The chemokine SDF-1, stromal cell-derived factor 1, attracts early stage B cell precursors via the chemokine receptor CXCR4. Eur J Immunol 1997;27:1788–93.
25. Hall J, Korach K. Stromal cell-derived factor 1, a novel target of estrogen receptor action, mediates the mitogenic effects of estradiol in ovarian and breast cancer cells. Mol Endocrinol 2003;17:792–803.
26. Sweeney T, Mailander V, Tucker A, et al. Visualizing the kinetics of tumor-cell clearance in living animals. Proc Natl Acad Sci USA 1999;96:12044–9.
27. Kijowski J, Baj-Krzyworzeka M, Majka M, et al. The SDF-1-CXCR4 axis stimulates VEGF secretion and activates integrins but does not affect proliferation and survival in lymphohematopoietic cells. Stem Cells 2001;19:453–66.
28. Pulaski B, Ostrand-Rosenberg S. MHC class II and B7.1 immunotherapeutic cell-based vaccine reduces spontaneous mammary carcinoma metastases without affecting primary tumor growth. Cancer Res 1998;58:1486–93.
29. Khanna C, Wan X, Bose S, et al. The membrane-cytoskeleton linker ezrin is necessary for osteosarcoma metastasis. Nat Med 2004;10:182–6.
30. Luzzi K, MacDonald I, Schmidt E, et al. Multistep nature of metastatic inefficiency: dormancy of solitary cells after successful extravasation and limited survival of early micrometastases. Am J Pathol 1998;153:865–73.
31. Wong C, Lee A, Shientag L, et al. Apoptosis: an early event in metastatic inefficiency. Cancer Res 2001;61:333–8.
32. Zhou Y, Larsen P, Hao C, Yong V. CXCR4 is a major chemokine receptor on glioma cells and mediates their survival. J Biol Chem 2002;277:49481–7.
33. Robinson S, Scott K, Wilson J, Thompson R, Proudfoot A, Balkwill F. A chemokine receptor antagonist inhibits experimental breast tumor growth. Cancer Res 2003;63:8360–5.
34. Goldberg-Bittman L, Neumark E, Sagi-Assif O, et al. The expression of the chemokine receptor CXCR3 and its ligand, CXCL10, in human breast adenocarcinoma cell lines. Immunol Lett 2004;92:171–8.
35. Tamamura H, Hori A, Kanzaki N, et al. T140 analogs as CXCR4 antagonists identified as anti-metastatic agents in the treatment of breast cancer. FEBS Lett 2003;550:79–83.
36. Kato M, Kitayama J, Kazama S, Nagawa H. Expression pattern of CXC chemokine receptor-4 is correlated with lymph node metastasis in human invasive ductal carcinoma. Breast Cancer Res 2003;5:R144–50.
37. Scotten C, Wilson J, Scott K, et al. Multiple actions of the chemokine CXCL12 on epithelial tumor cells in human ovarian cancer. Cancer Res 2002;62:5930–8.
38. Fernandis A, Prasad A, Band H, Klosel R, Ganju R. Regulation of CXCR4-mediated chemotaxis and chemoinvasion of breast cancer cells. Oncogene 2004;23:157–67.
39. Folkman J. Angiogenesis and apoptosis. Semin Cancer Biol 2003;13:159–67.
40. Datema R, Rabin L, Hincenbergs M, et al. Antiviral efficacy in vivo of the anti-human immunodeficiency virus bicyclam SDZ SID 791 (JM 3100), an inhibitor of infectious cell entry. Antimicrob Agents Chemother 1996;40:750–4.